CONTROL ORIENTATED SYNTHESIS OF ELECTROMAGNETIC SHUNT IMPEDANCES FOR VIBRATION ISOLATION [1]

S. Behrens [*,2] **A. J. Fleming** [*] **S. O. R. Moheimani** [*]

[*] *School of Electrical Engineering and Computer Science*
University of Newcastle, NSW 2308, Australia

Abstract: A typical passive mechanical isolation system utilizes a mass-spring-damper as a mechanical filter. Active isolation control systems typically include an electromagnetic transducer to develop the required control forces. In this paper, the technique of sensor-less active shunt control is applied to a mechanical isolation system. An electrical impedance is designed and connected to an electromagnetic transducer with a view to minimizing structural vibration. Standard control tools can be applied to design the required shunt impedance. The technique requires no additional feedback sensors. Vibration of an experimental isolation apparatus is heavily attenuated by the application of an active shunt impedance.

Keywords: isolation, electromagnetic, vibration, control, synthesis.

1. INTRODUCTION

The objectives of *damping* and *isolation* of noise and vibration are sometimes confused. In a few words, *damping* is regarded as the reduction of amplitude of the mechanical system within a limited bandwidth near the resonance frequency. While *isolation* is defined as supporting a static load within a particular bandwidth ω_c, and attenuation of high frequency components above ω_c, as shown in Figure 1.

A key example of an isolation system is active suspension control for automobiles (Choi *et al.*, 1998; Sohn *et al.*, 2000; Fukao *et al.*, 1999; Joo *et al.*, 2000; Ikenaga *et al.*, 2000; Smith and Wang, 2002; Gillespie, 1992). Normally an accelerometer, or force transducer, is used as a sensor while an electromagnetic transducer is used as an actuator.

Electromagnetic transducers can be used as sensors and actuators (Rao, 1995). Electromagnetic shunting control combines both the sensor and actuator together as *self-sensing* (Behrens *et al.*, 2003; Fleming *et al.*, 2003). By connecting an electrical impedance to the terminals of an electromagnetic coil, the relative mechanical velocity between the coil and magnet can be reduced. From a theoretical view point, the proposed control scheme is considered to be perfectly *collocated* (MacMartin, 1995), which improves the stability and robustness of the closed-loop system.

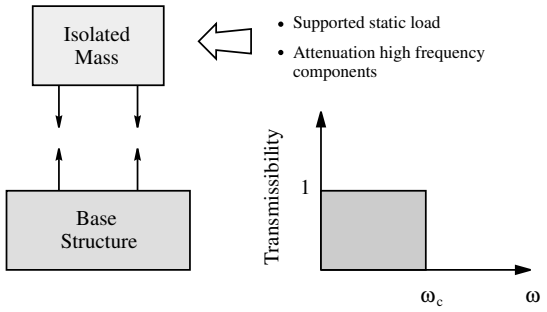

Fig. 1. Principle of an isolation system and isolation objectives.

In this paper, we will develop a sensor-less active shunt control for a simple mechanical isolation system. An electrical impedance is designed using standard control tools. To validate the proposed theoretical ideas, an active shunt impedance is applied experimentally to a simple electro-mechanical isolation apparatus.

[1] This research was supported by the Australian Research Council (ARC).
[2] sbehrens@ecemail.newcastle.edu.au

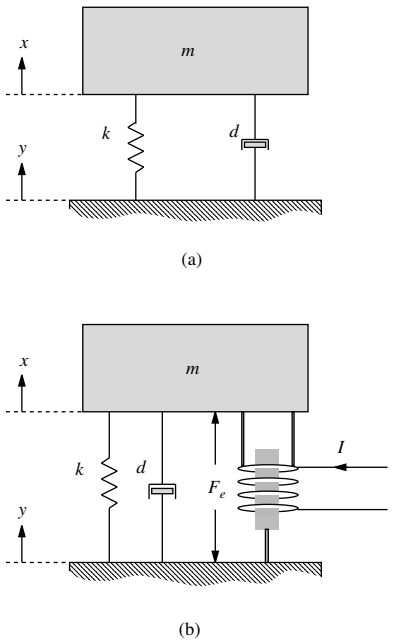

Fig. 2. Simple-mass-spring-damper isolation system: (a) unforced and (b) forced systems.

2. MODELLING

2.1 *Mechanical System*

Consider the simple isolation system shown in Figure 2 (a). The isolation system consists of a linear spring in parallel with a passive damper, where m is the mass, k and d are the stiffness and damping coefficients respectively. The equation of motion is defined as

$$m\ddot{x}(t) + d\dot{x}(t) + kx(t) = d\dot{y}(t) + ky(t), \quad (1)$$

where $(\cdot\cdot)$ and $(\cdot)$ denote the acceleration and velocity of $x(t)$ and $y(t)$. The resonance frequency of the mechanical system is $\omega_n = \sqrt{\frac{k}{m}}$ and the amount of damping is defined by the damping ratio ζ where $\frac{d}{m} = 2\zeta\omega_n$. The transfer function between the disturbance displacement y and the mass displacement x, alternatively, the disturbance velocity ϖ and the mass velocity v, is given by

$$T(s) \triangleq G_{yx}(s) = G_{\varpi v}(s) = \frac{\frac{2\zeta s}{\omega_n} + 1}{\frac{s^2}{\omega_n^2} + \frac{2\zeta s}{\omega_n} + 1}. \quad (2)$$

Equation (2) is commonly referred to as the *transmissibility ratio* $T(s)$. We can plot $T(s)$ against normalized frequency $\frac{\omega}{\omega_n}$ for various values of damping ratio ζ, as shown in Figure 3. Many interesting observations can be learned from Figure 3. They are:

(1) When the disturbing frequency coincides with the natural frequency of the system, an overshoot appears showing that the system vibrates at this frequency with high amplitudes.
(2) The frequency where the curve crosses over the 0 dB line is reached when the disturbing frequency is equal to $\omega_c = \sqrt{2}\omega_n$. This critical frequency is the point where the influence of vibration isolation begins.

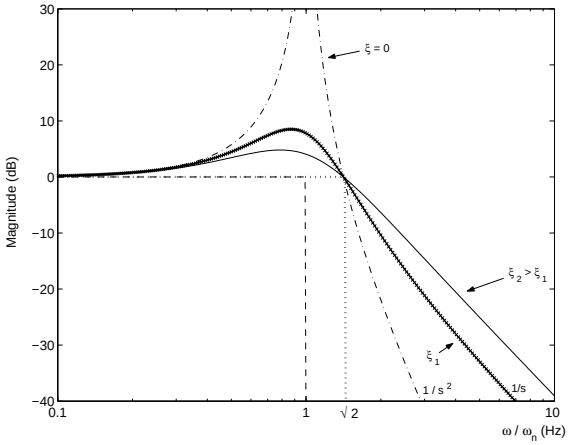

Fig. 3. Normalized transmissibility ratio $T(s)$ of a passive damper for various values of damping ratio ζ.

(3) At low frequencies, below the resonance of the system, the displacement of the sensitive payload follows faithfully the displacement of the disturbance source as if the isolator were infinitely rigid. However, at higher frequencies, greater than the resonance of the system, the curve rolls-off and the displacement of the payload decreases gradually while the disturbance is constant.
(4) When we increase the damping ratio ζ, the overshoot that appears at the natural frequency decreases but, unfortunately, the sharpness of the roll-off at high frequency decreases too.
(5) To maintain the sharp roll-off at high frequencies while decreasing the overshoot at the resonance, a control algorithm is needed.

From Figure 3, we can see that when $\zeta = 0$, the high frequency roll-off is $1/s^2$ (-40 dB/decade) while very large amplitude is seen near the natural frequency ω_n. On the other hand, when the damping ratio ζ is increased we reduce the overshoot at the resonance but we reduce also the roll-off to $1/s$ (-20 dB/decade). As a result, the design of a passive damper involves a trade-off between the resonance amplification and the high frequency attenuation.

From these observations we are motivated to design an active control scheme, which could possibly overcome a majority of these trade-offs and limitations.

2.2 *Composite System in General Form*

For the forced isolation problem, as shown in Figure 2 (b), a control force $F_e(t)$ is placed between the mass and the base. For this system, the equation of motion is

$$m\ddot{x}(t) + d\dot{x}(t) + kx(t) + F_e(t) = d\dot{y}(t) + ky(t).$$

The plant two-input-two-output model of the isolation system, P, is shown in Figure 4, where the disturbance velocity is referred to as $\varpi(t)$, $\varpi(t) = \dot{x}(t)$, and control force $F_e(t)$. The outputs of the plant are mass velocity as $v(t)$ and the relative velocity of the base and mass $r(t)$, $r(t) = v(t) - \varpi(t)$. That is,

$$\dot{\mathbf{x}}_p(t) = \begin{bmatrix} \frac{-d}{m} & \frac{-k}{m} \\ 1 & 0 \end{bmatrix} \mathbf{x}_p(t) + \begin{bmatrix} \frac{d}{m} & \frac{1}{m} \\ -1 & 0 \end{bmatrix} \begin{bmatrix} \varpi(t) \\ F_e(t) \end{bmatrix}$$

$$\begin{bmatrix} v(t) \\ r(t) \end{bmatrix} = \begin{bmatrix} 1 & 0 \\ 1 & 0 \end{bmatrix} \mathbf{x}_p(t) + \begin{bmatrix} 0 & 0 \\ -1 & 0 \end{bmatrix} \begin{bmatrix} \varpi(t) \\ F_e(t) \end{bmatrix}, \quad (3)$$

where the states are $\mathbf{x}_p(t) = [\, v(t) \;\; x(t) - y(t) \,]'$.

For the electromagnetic transducer system E having the following two-input-two-output system (Behrens *et al.*, 2003; Fleming *et al.*, 2003),

$$\dot{x}_e(t) = \begin{bmatrix} \frac{-R_e}{L_e} \end{bmatrix} x_e(t) + [\, c_{vv} \;\; -1 \,] \begin{bmatrix} r(t) \\ V_z(t) \end{bmatrix}$$

$$\begin{bmatrix} F_e(t) \\ I_z(t) \end{bmatrix} = \begin{bmatrix} \frac{-c_{if}}{L_e} \\ \frac{1}{L_e} \end{bmatrix} x_e(t), \quad (4)$$

where L_e and R_e are the inductance and resistance of the electromagnetic transducer respectively. Also, the coupling coefficients for the electromagnetic transducer are represented by c_{vv} and c_{if} , where $c_{vv} = \frac{V_e}{r}$ and $c_{if} = \frac{F_e}{I_z}$. Equation (4), can be represented in diagram form as shown in Figure 4.

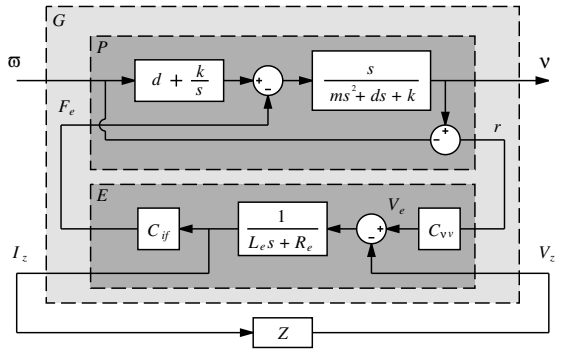

Fig. 4. Electro-mechanical isolation system G with subsystem P and E.

For the electromagnetic isolation system, we can combine systems P and E to obtain the following composite system G, where the dynamics of the transducer is introduced to the plant, as shown in Figure 4. The state-space representation of G, is

$$\begin{aligned} \dot{\mathbf{x}}_g(t) &= \mathbf{A}\mathbf{x}_g(t) + \mathbf{B_1}\varpi(t) + \mathbf{B_2}V_z(t) \\ v(t) &= \mathbf{C}_1\mathbf{x}_g(t) \\ I_z(t) &= \mathbf{C}_2\mathbf{x}_g(t) \end{aligned} \quad (5)$$

where

$$\mathbf{A} = \begin{bmatrix} \frac{-d}{m} & \frac{-k}{m} & \frac{-c_{if}}{mL_e} \\ 1 & 0 & 0 \\ c_{vv} & 0 & \frac{-R_e}{L_e} \end{bmatrix} \quad \mathbf{x}_g(t) = \begin{bmatrix} v(t) \\ x(t) - y(t) \\ x_e(t) \end{bmatrix}$$

$$\mathbf{B}_1 = \begin{bmatrix} \frac{d}{m} \\ \frac{-1}{m} \\ -c_{vv} \end{bmatrix} \quad \mathbf{B}_2 = \begin{bmatrix} 0 \\ 0 \\ -1 \end{bmatrix}$$

$$\mathbf{C}_1 = [\, 1 \;\; 0 \;\; 0 \,] \quad \mathbf{C}_2 = \begin{bmatrix} 0 & 0 & \frac{1}{L_e} \end{bmatrix}.$$

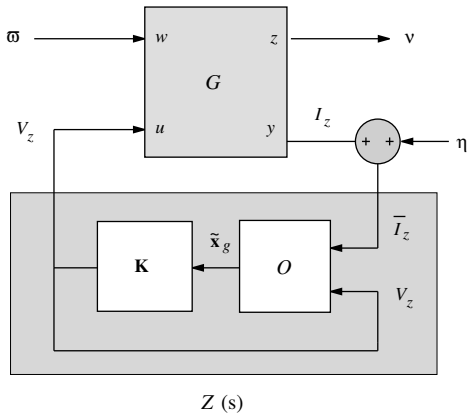

Fig. 5. The composite plant G controlled by $Z(s)$, an impedance consisting of the state-feedback controller K and Kalman filter O.

3. CONTROL DESIGN

The purpose of the controller would be to move specific poles of the system further into the left-half plane without affecting the zeros of the system. To achieve this, we need to design a controller that effectively add mechanical damping to the electro-mechanical system. This is achieved by allowing the damping term d of the open-loop matrix $\mathbf{A}$ to become $\tilde{d} = d + \alpha$, where α is some positive gain. That is, the effective closed-loop matrix $\tilde{\mathbf{A}}$ becomes

$$\tilde{\mathbf{A}} = \begin{bmatrix} \frac{-\tilde{d}}{m} & \frac{-k}{m} & \frac{-c_{if}}{mL_e} \\ 1 & 0 & 0 \\ c_{vv} & 0 & \frac{-R_e}{L_e} \end{bmatrix}. \quad (6)$$

Therefore, the desired closed-loop poles p are the eigenvalues of $\tilde{\mathbf{A}}$.

Now, given the system

$$\dot{\mathbf{x}}_g(t) = \mathbf{A}\mathbf{x}_g(t) + \mathbf{B_2}V_z(t) \quad (7)$$

and p of desired closed-loop pole locations, we can use Ackermann's formula (Kailath, 1980) to calculate a gain vector K such that the state-feedback $V_z(t) = -K\mathbf{x}_g(t)$ places the closed-loop poles at the locations p. In other words, the eigenvalues of $\mathbf{A} - \mathbf{B_2}K$ match the entries of p.

As state-feedback $V_z(t) = -K\mathbf{x}_g(t)$ is not implementable without full state measurement, a linear observer is required, as shown in Figure 5. It is possible, however, to derive a state estimate $\tilde{\mathbf{x}}_g(t)$ such that $V_z(t) = -K\tilde{\mathbf{x}}_g(t)$ remains optimal for the output-feedback problem. This state estimate is generated by the Kalman filter (Kailath, 1980)

$$\frac{d}{dt}\dot{\tilde{\mathbf{x}}}_g(t) = \mathbf{A}\tilde{\mathbf{x}}_g(t) + \mathbf{B}_2V_z(t) + \mathbf{L}(\bar{I}_z(t) - \mathbf{C}_2\tilde{\mathbf{x}}_g(t))$$

with inputs $V_z(t)$ (control) and $\bar{I}_z(t)$ (measurement). With the inclusion of measurement noise η, as shown in Figure 5, the system representation (5) becomes,

$$\begin{aligned} \dot{\mathbf{x}}_g(t) &= \mathbf{A}_g\mathbf{x}_g(t) + \mathbf{B_1}\varpi(t) + \mathbf{B_2}V_z(t) \\ v(t) &= \mathbf{C}_1\mathbf{x}_g(t) \\ I_z(t) &= \mathbf{C}_2\mathbf{x}_g(t) + \eta. \end{aligned}$$

The noise covariance data

$$E\{\varpi\varpi'\} = \mathbf{Q}_n \;\; E\{\eta\eta'\} = \mathbf{R}_n$$

determines the Kalman gain $\mathbf{L}$ through an algebraic Ricatti equation (Skogestad and Postlethwaite, 1996).

The Kalman filter is an optimal estimator when dealing with Gaussian white noise η. Specifically, it minimizes the asymptotic covariance

$$\lim_{t\to\infty} E\left\{[\mathbf{x}_g(t) - \tilde{\mathbf{x}}_g(t)]\,[\mathbf{x}_g(t) - \tilde{\mathbf{x}}_g(t)]'\right\} \qquad (8)$$

of the estimation error $\mathbf{x}_g(t) - \tilde{\mathbf{x}}_g(t)$.

Based on $\mathbf{Q}_n$ and $\mathbf{R}_n$ a Kalman observer that minimizes (8) can be found through the solution of an algebraic Ricatti equation (Skogestad and Postlethwaite, 1996). The ratio of $\mathbf{Q}_n$ to $\mathbf{R}_n$ essentially represents the confidence in the measured variable $I_z(t)$ and model G. In this work, $\mathbf{Q}_n$ and $\mathbf{R}_n$, are not quantified and simply treated as design parameters influencing the closed-loop pole locations, damping performance, and closed-loop stability.

4. EXPERIMENTAL VERIFICATION

To verify the modeling and design techniques presented in the previous sections, each method has been applied to an experimental electromechanical isolation system.

4.1 *Electromagnetic Apparatus*

To support the proposed electromagnetic shunt isolation technique, experiments were carried out on a simple electromagnetic isolation apparatus, as shown in Figure 6. The apparatus consist of five identical Jaycar Electronics [3] subsonic transducers Cat. XC-1008. Each transducer consists of a permanent toroid magnet, a coil, supporting frame, magnetic circuit and flexible supports, as shown in Figure 7 (a). Each transducer is mechanically equivalent to the electromagnetic mass-spring-damper, as shown in Figure 7 (b).

By connecting electromagnetic transducers together, as shown in Figures 6 and , where isolation transducer is the isolated mass-spring-damper system and base transducers as the base disturbance, we obtain a simple experimental isolation system. Note that the base transducers are connected to ground. For our case a Newport© RS 3000 optical table was utilized.

Now, a disturbance current $I_d(s)$ is applied to the base transducers as a base disturbance. To measure the transmissibility ratio $T(s)$, two B&K© accelerometers were used to measure the applied base velocity $\varpi(s)$, accelerometer 2, and the isolated mass velocity $v(s)$, accelerometer 1, as shown in Figure 8.

Experimental parameters for the isolated system are the isolated mass $m = 0.4\ kg$, the damping constant $d = 2.18\ Nsm^{-1}$, the spring constant $k = 29.4\ kNm$, the electro-mechanical coupling $c_{vv} = 3.65$ and $c_{if} = 3.6$, the coil inductance $L_e = 0.320\ mH$, and the coil resistance $R_e = 4.0\ \Omega$.

[3] www.jaycar.com.au

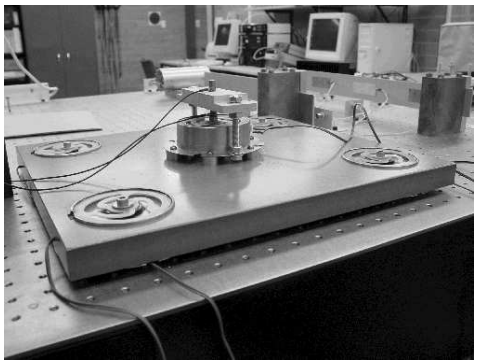

Fig. 6. Isolation experimental apparatus.

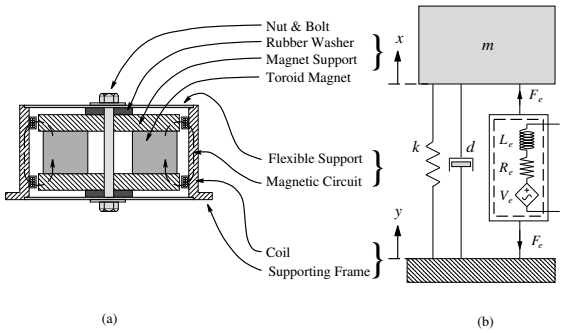

Fig. 7. Electromagnetic transducer: (a) cross section, and (b) mechanical equivalent.

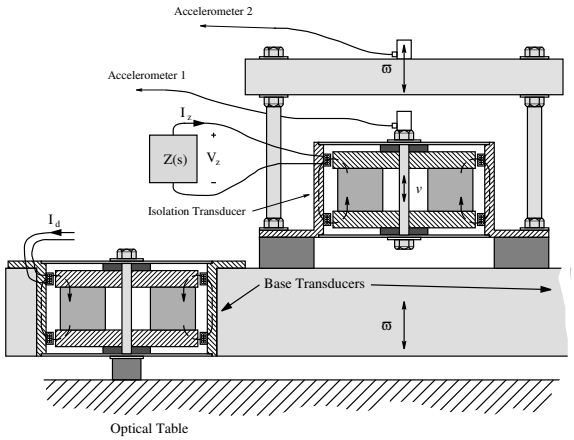

Fig. 8. Quarterview section of the experimental isolation apparatus. Isolation transducer is shunted by $Z(s)$, whilst applying a disturbance current $I_d(s)$ to base transducers.

4.2 *Power Amplifier and Instrumentation*

In order to implement the arbitrary shunt impedance resulting from the control design, a power amplifier was developed capable of driving differential terminal voltages. During operation the device is capable of instrumenting the respective load current.

A current-controlled-voltage-source (CCVS) is shown in Figure 9. In Figure 9, within the high frequency bandwidth of the control loop, the reference potential V_{ref} appears across the load, i.e. we have a unity gain voltage amplifier. The additional resistance and differ-

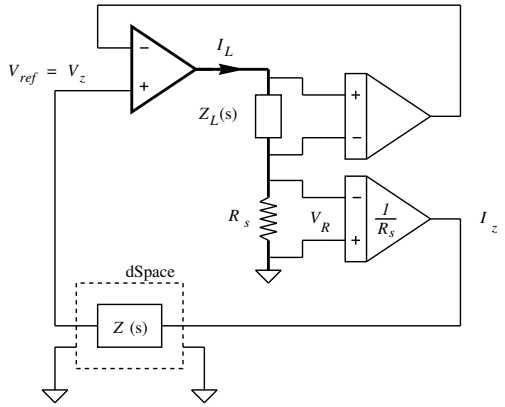

Fig. 9. The simplified schematic of a differential voltage feedback amplifier. The load impedance $Z_L(s)$ represents the electromagnetic coil.

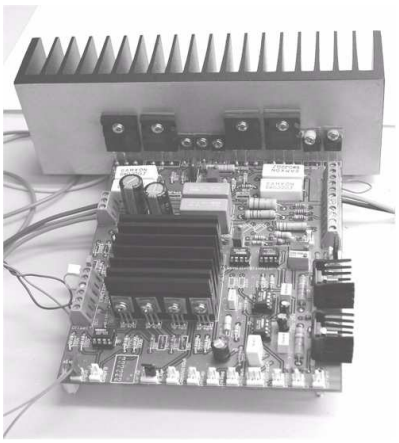

Fig. 10. Practical implementation of a voltage amplifier with current instrumentation.

ential amplifier generate the current measurement V_R with gain R_s V/A.

A practical implementation of the amplifier is shown in Figure 10. The device is capable of ± 200 V operation at a maximum DC current of ± 32 $Amps$. Further analysis and a more detailed discussion of the implementation can be found in (Fleming and Moheimani, 2002). A dSpace© 1005 based system is used to implement the required impedance $Z(s)$ transfer function.

4.3 *Verification*

Figure 11 shows the instrumentation and driver gains associated with the underlying electromechanical system. The voltages V_1 through V_4 represent the signals applied to, or measured from, the power amplifiers and instrumentation. The gain and units associated with each signal are $a_1 = 1.0\ ms^{-1}/V$, $a_2 = 1.0\ V/ms^{-1}$, $a_3 = 1.0\ V/V$ and $a_4 = 1.0\ V/A$. The actual electrical shunt impedance applied to the coil is related to the controller through the gains a_3 and a_4, specifically,

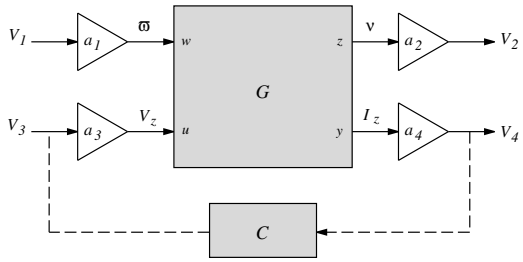

Fig. 11. External gains associated with the amplifier and instrumentation.

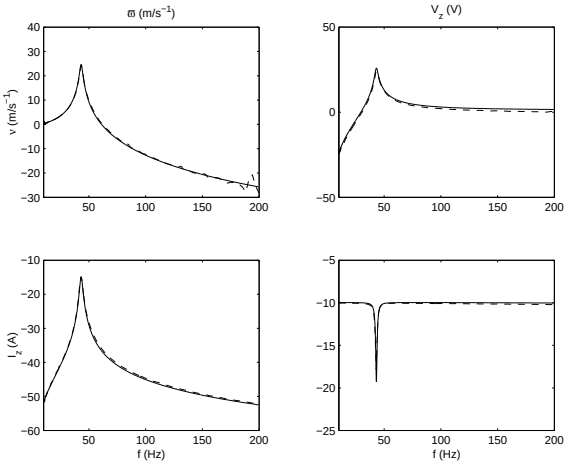

Fig. 12. The simulated (—), and experimental (−−), magnitude frequency response.

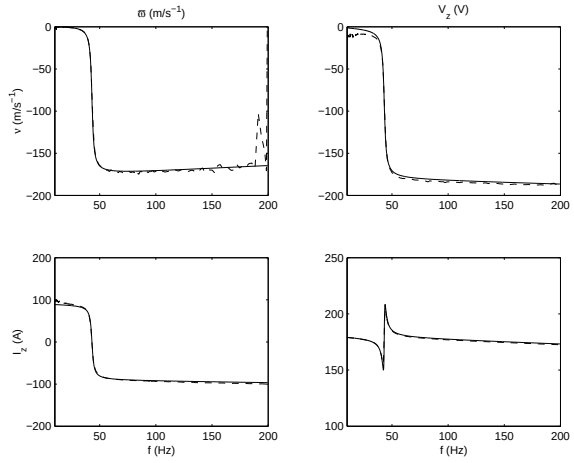

Fig. 13. The simulated (—), and experimental (−−), phase frequency response.

$$Z_c(s) = \frac{V_z(s)}{I_z(s)} = a_3 C(s) a_4. \tag{9}$$

To validate the proposed model for the electromechanical isolation system, experimental frequency response data was obtained. The magnitude and phase frequency responses are shown respectively in Figures 12 and 13. From Figures 12 and 13, we can see a good correlation between the analytical model and experimental data. Therefore, validating the proposed model of the electromagnetic isolation apparatus.

As discussed in Section 3, we can use the Matlab© place command to design a state-feedback controller

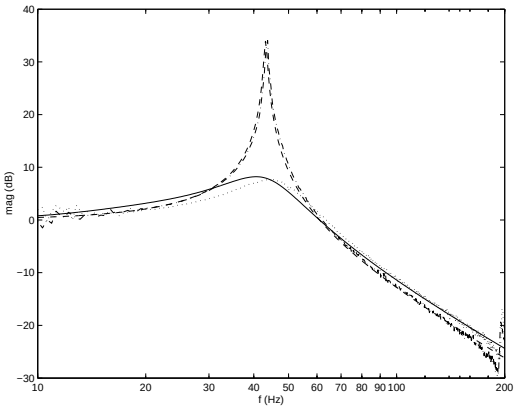

Fig. 14. Magnitude $T(s)$ response of the isolation system. Simulated open- ($--$), closed- (—), and experimental open- ($-\cdot-$) and closed-loop ($\cdots$).

K. Assuming $\alpha = 46$, the state-feedback controller is $K = [\, 38.9 \;\; -300.5 \;\; -115.0 \,]$.

An observer is required to estimate the system states from the measured shunt current I_z. A Kalman observer was designed to estimate the system state $\tilde{\mathbf{x}}_g(t)$ utilizing the measured shunt transducer current I_z and control signal V_z. Referring to Section 3, the disturbance and output noise process covariance matrices, $\mathbf{Q}_n$ and $\mathbf{R}_n$, were chosen to be 3 and 0.1 respectively. Such a weighting, although not quantitative, expresses a moderate confidence in the fidelity of the measured variable I_z.

By concatenating the K gain matrix and Kalman observer, and compensating for the system gains a_3 and a_4, the actual impedance presented to the shunt transducer, is

$$Z_c(s) = \frac{-2.448\times10^4 s^2 - 2.193\times10^8 s + 1.308\times10^{11}}{s^3 + 6.345\times10^4 s^2 + 9.247\times10^7 s - 4.219\times10^{10}}.$$

The open- and closed-loop transfer function from an applied disturbance to the measured vibration can be seen in the frequency domain, Figure 14. The resonant peak has been experimentally damped by $26.2\ dB$.

5. CONCLUSION AND DISCUSSION

In this paper, the connection of electrical impedance to the terminals of an electromagnetic isolation system was shown to be equivalent to implementing a standard feedback controller. A method using pole placement and a Kalman observe for the design of appropriate designed impedance is proposed. While designing the controller two important objectives were considered, they are; resonant peak damping and high frequency attenuation. Both of these objectives where achieved through simulation and experimentation on a simple isolation apparatus.

Current and future work involves both the exploration of the control theory associated with the synthesis step and inclusion of uncertainty in the plant model to guarantee robustness and stability.

6. REFERENCES

Behrens, S., A. Fleming and S. O. R. Moheimani (2003). Electromagnetic shunt damping. In: *IEEE/ASME International Conference on Advanced Intelligent Mechatronics 2003*. Kobe, Japan.

Choi, J. W., Y. B. Seo, W. S. Yoo and M. H. Lee (1998). Lqr approach using eignstructure assignment with an active suspension control application. In: *Proc. IEEE International Conference on Control Applications*. Trieste, Italy. pp. 1235–1239.

Fleming, A. and S. O. R. Moheimani (2002). Improved current and charge amplifiers for driving piezoelectric loads, and issues in signal processing design for synthesis of shunt damping circuits.. *Journal of Intelligent Material Systems and Structures*.

Fleming, A., S. Behrens and R. Moheimani (2003). Active $\mathcal{H}_2$ and $\mathcal{H}_\infty$ shunt control of electromagnetic transducer. In: *IEEE Conference on Decision and Control*.

Fukao, T., A. Yamawaki and N. Adachi (1999). Nonlinear and $\mathrm{h}\inf$ control of active suspension systems with hydraulic actuators. In: *Proc. IEEE Conference on Decision and Control*. Phoenix, Arizona USA. pp. 5125–5128.

Gillespie, T. D. (1992). *Fundamentals of Vehicle Dynamics*. Society of Automotive Engineers.

Ikenaga, S., F. L. Lewis, J. Campos and L. Davis (2000). Active suspension conrol of ground vehicle based on a full-vehicle model. In: *Proc. IEEE American Control Conference*. Chicago, Illinois USA. pp. 4019–4024.

Joo, D. S., N. Al-Holou, J. M. Weaver, Lahdhiri and F. Al-Abbas (2000). Nonlinear modeling of vehicle suspenesion systems. In: *Proc. IEEE American Control Conference*. Chicago, Illinois USA. pp. 115–118.

Kailath, T. (1980). *Linear Systems*. Printice-Hall. Upper Saddle River, NJ 07458.

MacMartin, D. G. (1995). Collocated structural control: motivation and methodology. In: *Proc. IEEE International Conference on Control Applications*. Albany, New York USA. pp. 1092–1097.

Rao, S. S. (1995). *Mechanical Vibrations*. 3rd ed.. Addison-Wesley Publishing Company.

Skogestad, S. and I. Postlethwaite (1996). *Multivariable Feedback Control*. John Wiley and Sons.

Smith, M. C. and F. Wang (2002). Controlle parameterization for disturnbance response decoupling: Application to vehicle active suspension control. *IEEE Transactions on Control Systems Technology* **10**(3), 393–407.

Sohn, H. C., K. S. Hong and J. K. Hedrick (2000). Semi-active control of the macpherson supension system: Hardware-in-the-loop simulations. In: *Proc. IEEE International Conference on Control Applications*. Anchorage, Alaska USA. pp. 982–987.